Experimental characterization and 3D simulations of turbulent flames assisted by nanosecond plasma discharges

Victorien P Blanchard, Yacine Bechane, Nicolas Q Minesi, Stéphane Q.E. Wang, Benoît Fiorina, Christophe O Laux

Combustion and Flame 270 (2024) 113709

Contents lists available at ScienceDirect

Combustion and Flame

journal homepage: www.sciencedirect.com/journal/combustion-and-flame

Experimental characterization and 3D simulations of turbulent flames assisted by nanosecond plasma discharges

Victorien P. Blanchard *, Yacine Bechane, Nicolas Q. Minesi, Stéphane Q.E. Wang, Benoît Fiorina, Christophe O. Laux

Laboratoire EM2C-CNRS, CentraleSupélec, Université Paris Saclay, 3 rue Joliot-Curie, 91190 Gif-sur-Yvette, France

ARTICLE INFO

Keywords:
Plasma-assisted combustion
Nanosecond discharges
Large Eddy Simulation
OH LIF
Temperature measurements
Phenomenological nanosecond discharge model

ABSTRACT

This paper presents quantitative experimental data generated for the validation of plasma-assisted combustion (PAC) simulations. These data are then used to validate the phenomenological model of Castela et al. They are also useful to test other PAC models. In the experiment presented here, Nanosecond Repetitively Pulsed (NRP) discharges are applied to a lean-premixed turbulent methane-air flame initially near the lean blow-off limit. The discharges significantly enhance the combustion and stabilize the flame after a few pulses. Electrical and optical diagnostics are employed to extensively quantify the transient and steady state of the plasma-stabilization process. The flame shape is characterized by OH* chemiluminescence imaging. In the discharge region, OH density profiles are obtained by 1D laser-induced fluorescence, and the gas temperature is measured by optical emission spectroscopy measurements. The local gas temperature increases by 1250 K, and the OH number density rises sevenfold when NRP discharges are applied. These results evidence the cumulative thermal and chemical effects of NRP discharges, which are especially challenging to replicate numerically. A Large Eddy Simulation (LES) of the experiment is performed. Combustion chemistry is modeled by an analytically reduced mechanism, while the plasma discharge is described by the low-CPU cost phenomenological model of Castela et al., which aims to capture the main thermal and chemical effects induced by the discharges. The model of Castela et al. is validated in the burnt gases by the remarkable agreement between the simulations and the experiments regarding the flame shape, the local gas temperature, and the OH number density. More generally, this work demonstrates the relevance of simplified plasma models in LES solvers to simulate complex plasma-assisted burners.

1. Introduction

For decades, carbon-based fossil fuels have provided more than 80 % of the world's total energy supply [1]. To achieve net zero CO_2 emissions by 2050, the shift to a clean energy economy is required. However, many industrial combustion processes cannot be replaced by carbon-free electrification. Promising alternatives include low-carbon fuels such as biofuels, synthetic fuels, hydrogen, or ammonia, but their combustion is still responsible for the emissions of pollutants such as carbon monoxide, nitric oxides (NO_x), sulfur oxides, soot, and particulate matter. A strategy to mitigate pollutant formation consists in decreasing the flame temperature by burning lean-premixed fuel-air mixtures. Lean-premixed combustion, however, is subject to instabilities and blow-off that are detrimental to operability in most applications [2].

A promising way to extend the flame stability limit is to apply electrical pulses [3–5], especially Nanosecond Repetitively Pulsed (NRP) discharges [6–8]. These nonequilibrium discharges efficiently produce reactive species and promote combustion at a low power budget, typically 0.1–1 % of the flame thermal power [9–16]. It was shown in previous works that nanosecond discharges can significantly extend the lean blow-off limits of a bluff-body burner [14] and of swirl-stabilized burners [15,17–21]. The ability of nanosecond discharges to stabilize lean flames was also experimentally demonstrated for both gaseous and liquid fuels [18], for thermal powers up to 100 kW [15,19,21], and pressures up to 5 bar [20,22].

The effects of NRP discharges on flame stability are still an ongoing research subject. Simulations are carried out to identify the mechanisms of temperature increase, the pathways of radicals formation, and their interaction with the fuel and oxidizer molecules [9,23–32]. However, plasma-assisted combustion (PAC) simulations with detailed chemistry

* Corresponding author.
E-mail address: victorien.blanchard@centralesupelec.com (V.P. Blanchard).

https://doi.org/10.1016/j.combustflame.2024.113709
Received 24 July 2023; Received in revised form 26 August 2024; Accepted 28 August 2024
Available online 23 October 2024

are mainly limited to 0D or 1D configurations because of computational cost constraints. Detailed plasma and combustion kinetics, along with the resolution of the Poisson and fluid equations, were incorporated in 2D numerical simulations of H_2-air ignition by a nanosecond discharge [33,34]. These studies are essential to investigate the interaction of the discharge with the gas and the non-uniform effects, but their implementation remains computationally prohibitive when simulating repetitive discharges. To circumvent this problem, Bak et al. [35] performed 2D simulations of a laminar methane-air flame stabilized by NRP discharges at 30 kHz, assuming a homogeneous electric field. However, coupling a 3D turbulent combustion solver with a plasma discharge solver is still challenging, and simulations are computationally prohibitive when applying several discharges in sequence.

To overcome these limitations, Castela et al. [36] developed a reduced analytical model to simulate the effects of NRP discharges. Their model predicts the fraction of the discharge energy spent on fast gas heating and fast dissociation of O_2 at the nanosecond time scale, and on slow gas heating at the microsecond time scale [11,28]. Such reduced models are necessary to perform plasma-assisted combustion simulations in industrial applications where accurate and reliable numerical tools are needed to design innovative combustion chambers and plasma reactors. Initially applied to study the plasma-induced ignition of a quiescent combustible mixture [37], the model of Castela et al. was recently implemented in a Large Eddy Simulation (LES) solver to study the ignition and enhancement of premixed turbulent methane-air flames by a series of nanosecond discharges [38–40]. Additional simulations using Castela et al.'s model were performed by Malé et al. [12] to study the ignition of CH_4-H_2-air mixtures diluted with hot combustion products in the second stage of a sequential burner. Their results showed a significant improvement of the combustion efficiency near blow-off thanks to NRP discharges. Malé et al. also performed 0D kinetic simulations and found the model of Castela et al. to be in good agreement with the atomic oxygen mass fraction and the temperature evolution predicted by their simulations with detailed plasma chemistry. In Ref. [41], detailed plasma kinetics simulations were performed by Barléon et al. to extend the model of Castela et al. to a lean premixed methane-air flame at an equivalence ratio of 0.8. These simulations predicted an increase in temperature and radicals similar to the results obtained with Castela et al.'s model. However, although used in several works [12,37–39], the plasma-assisted combustion model developed by Castela et al. has not been validated yet through quantitative comparisons against experiments.

In general, the validation of a model requires a wide range of experimental conditions, and a single experiment is not sufficient to fulfil this task. For instance, ignition experiments aim to initiate the combustion chain-branching reactions efficiently and produce an ignition kernel that can further develop [42,43]. A few discharges are usually enough for ignition to occur. On the other hand, plasma-assisted stabilization of lean flames is expected to sustain these chain-branching reactions in conditions where they usually terminate without plasma. The stabilization is achieved by applying discharges continuously at a repetition frequency of a few tens of kHz. Steady-state experiments can test a model in continuous (forced regime) conditions but are not suitable for testing the ability of the model to reproduce the effect of a single discharge or a reduced number of discharges.

The first goal of this study is to generate experimental data in a turbulent plasma-assisted flame to validate PAC models. We define a reference experiment to assess not only the ability of a model to reproduce the effects of a few discharges, but also to reproduce steady-state conditions when discharges are applied continuously. A burst of nanosecond discharges is applied to a lean-premixed turbulent methane-air flame initially near the lean blow-off limit. Without discharges, the flame is relatively small and referred to as "weak flame". The NRP discharges progressively enhance the weak flame until a steady, stable flame is obtained. The impact of the discharges on the flame is characterized in terms of flame shape, temperature, and OH distribution in the vicinity of the discharges. This experiment thus allows testing models at both short time scales, i.e., transient effects, and long time scales, i.e., steady-state conditions.

The second goal of this study is to assess the ability of 3D LES incorporating the model of Castela et al. to reproduce the driving effects of nanosecond discharges on flame stabilization in the reference experiment.

This paper is organized as follows. Section 2 describes the experimental setup as well as the electrical and optical diagnostic techniques. Section 3 describes the numerical modeling. In Section 4, comparisons between experimental and numerical results are presented, with a focus on the evolution of flame shape, temperature, and OH number density.

2. Experimental setup and diagnostics

2.1. Experimental setup

Experiments are carried out with the Mini-PAC bluff-body burner extensively described in our previous work [44–48] and represented in Fig. 1. Methane and air are premixed in a chamber before being supplied at the bottom of the burner. The flame is anchored by a cylindrical bluff body aligned concentrically within the annular injection duct. The inner and outer diameters of the annular duct are 10 mm and 16 mm, respectively. The residence time in the recirculation zone created by the bluff body is long enough to stabilize the turbulent flame. The air flowrate is 16 Nm^3/h, and the methane flow rate is 1.34 Nm^3/h. For the equivalence ratio chosen in this experiment, $\Phi = 0.8$, the theoretical flame thermal power is 13.3 kW. The bulk flow velocity is about 43 m s^{-1}, which gives a Reynolds number based on the hydraulic diameter of $Re_D = 1.6 \times 10^4$. The flow is thus in a fully developed turbulent regime at the outlet of the injection duct.

The 2-mm vertical grounded cathode is centered on top of the bluff body, and the horizontal anode is located 5 mm above. Nanosecond discharges are generated across the 5-mm gap by 10-ns duration high-voltage pulses delivered by a pulse generator (FID Technology model FPG 10–30NM10). The deposited energy at steady state is fixed at 1.8 mJ per pulse and the discharges are applied at 20 kHz. The plasma-to-flame power ratio is therefore 0.3 %. Photographs of the flame without and with plasma are shown in Fig. 2.

2.2. Electrical measurements

The setup for electrical measurements is presented in Fig. 4 and is similar to the one presented in Ref. [44]. Voltage and current traces are measured with electrical probes (Lecroy PPE 20 kV and Pearson current

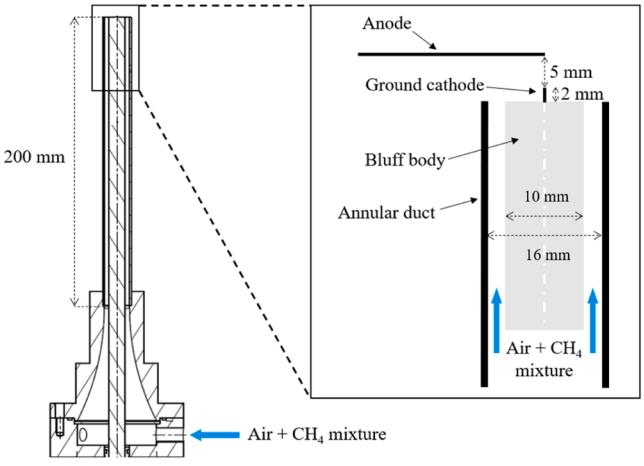

Fig. 1. Schematic of the bluff-body burner with electrodes. Reproduced from [47].

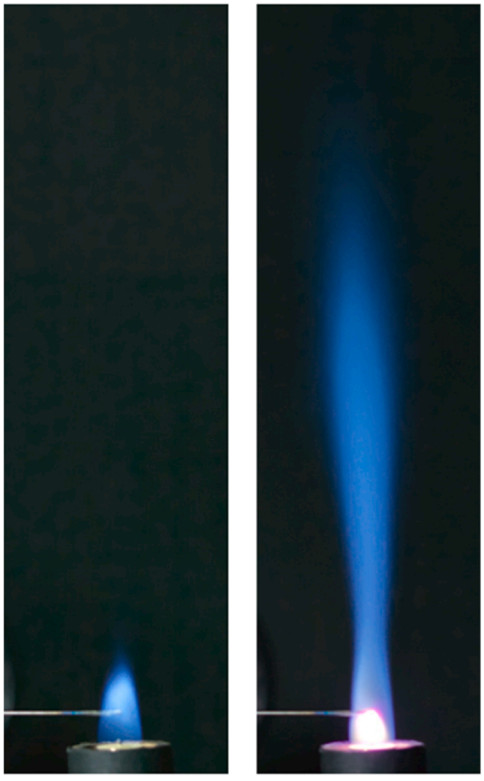

Fig. 2. Photographs in real colors of the lean methane-air flame at $\Phi = 0.8$ without (a) and with (b) 1.8-mJ NRP discharges applied at 20 kHz. The inter-electrode gap is 5 mm.

monitor model 6585) connected to an oscilloscope (TeledyneLecroy HDO 6104) to monitor the energy deposited by each discharge pulse. Fig. 3 shows the average current and voltage traces of the high-voltage

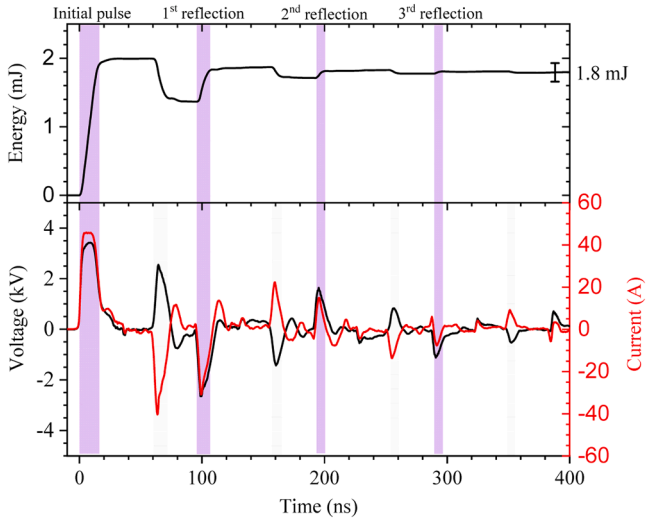

Fig. 3. Current (red) and voltage (black) traces measured halfway along the coaxial cable and resulting energy. The traces are obtained from an average of 10 000 samples. The error bar corresponds to one standard deviation of the energy measurement. The shaded areas correspond to the pulses incident on and reflected from the plasma (purple for incident pulses traveling from the pulser to the plasma, and grey for reflected pulses traveling back from the plasma to the pulser).

pulse along with the resulting energy when discharges are applied continuously at 20 kHz. The probes are located halfway on the 7-m long coaxial cable connecting the pulser to the electrode (see Ref. [44] for more details on the energy measurement). Due to the impedance mismatch between the interelectrode gap and the coaxial cable, part of the incident pulse is reflected and travels back to the pulse generator, where a second reflection occurs. As the incident and reflected pulses carry energy in opposite directions, these successive reflections cause a non-monotonic energy evolution. About 75 % of the total energy is deposited by the first incident pulse and the remaining energy is deposited within 300 ns by the reflections. The total energy dissipated into the plasma is 1.8 mJ at steady state. Note also that, due to the reflection at the electrode, the voltage applied across the interelectrode gap is twice the incident voltage (3.4 kV) shown in Fig. 3.

2.3. Flame imaging

OH* chemiluminescence images of the flame are recorded using an ICCD camera (Princeton Instruments, PI-MAX-512-T, 18/G/II) fitted with a UV-Nikkor 105 mm lens (f /4.5) and an interference bandpass filter (Asahi Spectra Optical Filters ZHQA310) centered at 310 nm (FWHM = 10 nm) to collect the spontaneous emission of the OH(A-X) transition. Images are acquired with a 48-μs time gate between consecutive discharges and a delay of 1 μs after the discharge to avoid direct discharge emission. All OH* chemiluminescent intensity images presented in this work are obtained from an average of 1000 samples.

2.4. Gas temperature measurements

The gas temperature is measured during each pulse using Optical Emission Spectroscopy (OES) of the N_2(C→B) (0,2) vibrational band. The relation between the gas temperature and the rotational temperature of N_2(C) was discussed in Refs. [11,44,49–51]. During a nanosecond pulse, N_2(C) is mainly populated from the ground electronic state of N_2 by electron-impact reactions. Because the rotational number is conserved through these reactions, on time scales shorter than the rotational-translation relaxation time, the rotational temperature of N_2(C), $T_{rot,N_2(C)}$ is proportional to the rotational temperature of N_2(X), $T_{rot,N_2(X)}$. The proportionality constant is equal to the ratio of the rotational constants, denoted θ^X_{rot} and θ^C_{rot}. Furthermore, Refs. [11,49] showed that the rotational temperature of N_2(X) is equilibrated with the gas temperature T_{gas}. At longer time scales, when rotational relaxation occurs, $T_{rot,N_2(C)}$ relaxes to T_{gas}. Thus, during a nanosecond pulse, we have the following general relation:

$$T_{rot,N_2(C)} \leq T_{gas} = T_{rot,N_2(X)} \leq T_{rot,N_2(C)} \times \frac{\theta^X_{rot}}{\theta^C_{rot}} = 1.095 \times T_{rot,N_2(C)} \quad (1)$$

It follows that the rotational temperature of N_2(C) is always within 10 % of the gas temperature during the pulse [11,49,51]. Furthermore, as shown in Ref. [51], rotational relaxation does not affect the rotational temperature of N_2(C) at the beginning of a nanosecond pulse. Thus, the gas temperature at the early times following each pulse can be obtained from the following relation:

$$T_{gas} = 1.095 \times T_{rot,N_2(C)} \quad (2)$$

The rotational temperature of N_2(C) is measured by OES with the experimental setup presented in Fig. 4. The spectra are acquired with a monochromator (Acton SpectraPro 2500i) coupled to an ICCD camera (Roper Scientific PI-MAX-512-T, 18/G/II). The discharge emission is collected with two plano-convex lenses of 100-mm focal length. A longpass interference filter with a cut-off wavelength at 300 nm (UV Melles Griot 03 FCG 121 WG 305) is inserted into the optical path to reject second-order emission of species emitting in the UV. The width of the entrance slit of the spectrometer is 75 μm. Spectra are acquired using a 1200-gr/mm grating blazed at 300 nm or a 2400-gr/mm grating

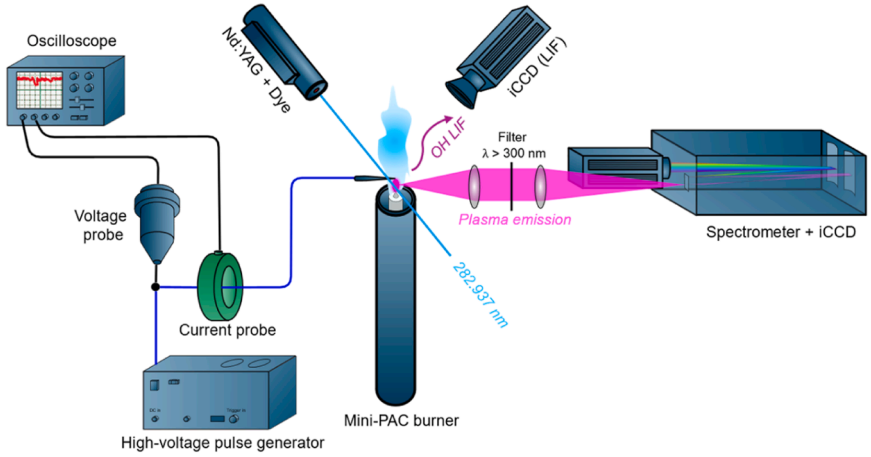

Fig. 4. Schematic of bluff-body burner and experimental setup for electrical and optical diagnostics.

blazed at 150 nm, yielding spectral resolutions of 0.142 nm and 0.065 nm, respectively. Experimental spectra are collected with a 2-ns time gate with a few hundred on-CCD accumulations depending on the intensity of the signal. The spectra are calibrated in intensity using an integrating sphere (Gooch & Housego OL 455–4–2) traceable to NIST standards. Experimental spectra of the N_2(C→B) (0,2) vibrational bands are fitted with the line-by-line radiation code SPECAIR [52,53] to determine the rotational temperature during the burst of discharges as done in [54]. The measurements presented in this paper correspond to the plasma emission in the middle of the 5-mm interelectrode gap.

For each discharge, spectra of the N_2(C→B) (0,2) vibrational band are acquired with 1-ns steps to track the evolution of the rotational temperature of N_2(C). Fig. 5 shows a typical experimental spectrum fitted using SPECAIR [52,53]. The uncertainty in the rotational temperature, estimated from the fit sensitivity, is typically 200 K, as shown in Fig. 5. As an example, Fig. 6 plots the rotational temperature evolution during the 10^{th} discharge of the burst. For this discharge, we measure a temperature increase of approximately 350 K within 15 ns, mostly at the end of the pulse. Time $t = 0$ ns is defined as the rising half-maximum of the discharge broadband emission during the high-voltage pulse. The measurements stop at $t = 14$ ns when the N_2(C) number density is too low for the emission spectrum to be fitted properly.

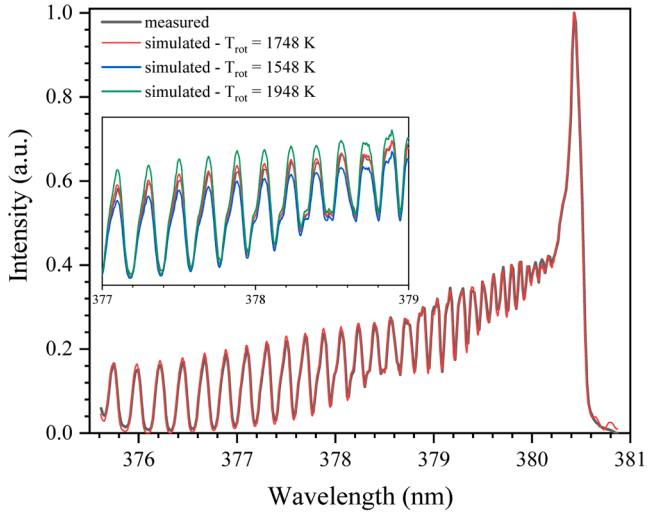

Fig. 5. Determination of the rotational temperature of N_2(C) by fitting the experimental spectrum with SPECAIR. The best fit is for T_{rot} = 1748±200 K. The fit sensitivity is illustrated by the two synthetic spectra at T_{rot} = 1548 K and 1948 K in the inset.

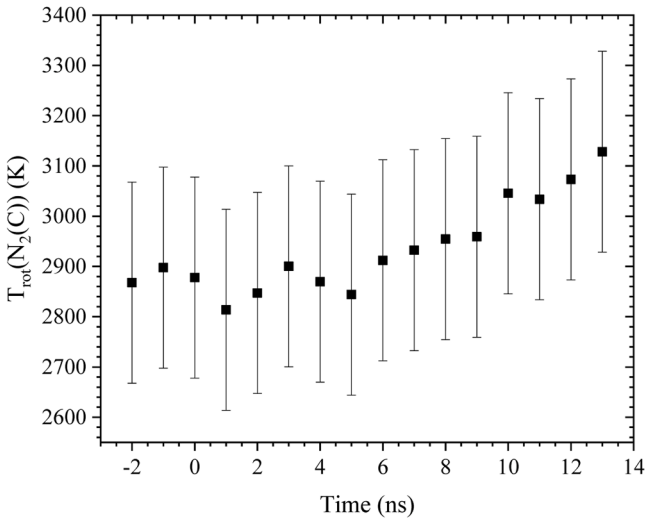

Fig. 6. Evolution of the rotational temperature of N_2(C) during the 10^{th} discharge of the burst. Spectra are measured in the middle of the interelectrode gap.

2.5. OH laser-induced fluorescence

The OH radicals produced after each discharge are measured by Laser-Induced Fluorescence (LIF). The experimental setup is extensively described in [49] and briefly presented here. The frequency-doubled output (532 nm) of a Nd:YAG laser (Continuum Precision) is used to pump a dye laser (Continuum ND6000 with rhodamine 590) at 10 Hz. The frequency-doubled output of the dye laser is then tuned to excite the $Q_2(3)$ transition of OH[($X^2\Pi_i$,v''=0)→($A^2\Sigma^+$,v'=1)] at 282.937 nm [55]. The laser beam is focused with a plano-convex lens (f = 15 cm) and the beam waist diameter is approximately 0.2 mm. The energy of the 10-ns laser pulse is set to 22 mJ, corresponding to a fluence of about 1.8 GW/cm^2. This level of fluence corresponds to the saturated regime, as experimentally verified in Fig. 7 in the non-assisted weak flame (Fig. 2a) above a laser pulse energy of 15 mJ.

A two-level model is used to interpret the measured fluorescence signals [56]. Assuming an equilibrium composition at the adiabatic flame temperature of a stoichiometric CH_4-air flame, the quenching lifetime of OH(A) is estimated with the rate constants of Ref. [50] to be about 1 ns, which is smaller than the laser pulse duration (12 ns). Thus, the collected fluorescence signal is at steady state in the saturated regime and is proportional to the OH(X, v''=0, J''=3) number density.

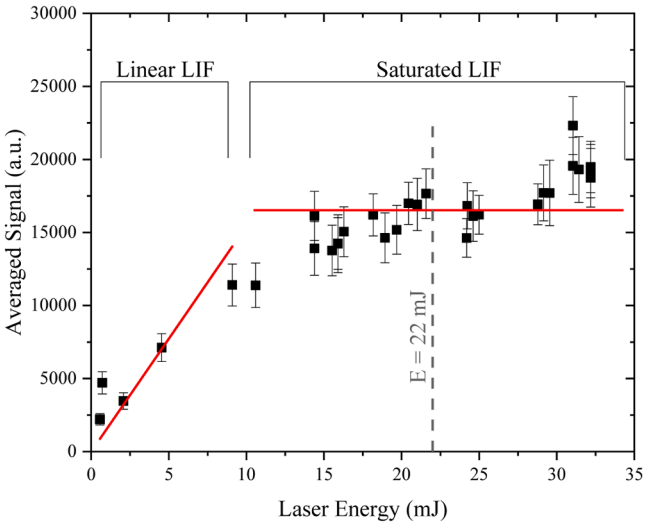

Fig. 7. Saturation curve of the LIF signal in the non-assisted flame.

The laser beam is adjusted to cross the discharge axis right in the middle of the interelectrode gap, 2.5 mm from the cathode and the anode, as shown in Fig. 8. The fluorescence signal is collected perpendicularly to the laser beam using an ICCD camera (Princeton Instruments, PI-MAX-512-T, 18/G/II) fitted with a UV-Nikkor 105 mm lens (f /4.5) and an interference bandpass filter (Asahi Spectra Optical Filters ZBPA310) centered at 310 nm (FWHM = 11 nm). The discharge, the laser, and the camera are synchronized using a gate-and-delay generator (BNC model 575). The camera gate is synchronized with the laser pulse and set to 12 ns. The LIF measurements are taken 45 µs after each pulse, i.e., near the end of the 50 µs interval between consecutive pulses, in order to avoid collecting the emission of the discharge.

In the saturated regime, the fluorescence signal is proportional to the density in the lower state pumped by the laser, OH($X^2\Pi_i$,v"=0, J"=3). Therefore, to obtain experimental OH profiles representative of the total number density of OH($X^2\Pi_i$), the profiles of OH($X^2\Pi_i$,v"=0, J"=3) are corrected by the temperature profiles using Eq. (3):

$$\frac{OH\left(X^2\Pi_i, v''=0,\ J''=3\right)}{OH\left(X^2\Pi_i\right)} = \frac{(2J''+1)\exp\left(-J''(J''+1)\theta_{rot,OH}/T\right)}{T/\theta_{rot,OH}}\left(1-\exp\left(-\frac{\theta_{vib,OH}}{T}\right)\right) \quad (3)$$

where $\theta_{rot,OH} = 27$ K, $\theta_{vib,OH} = 5378$ K [57]. The temperature profiles are obtained from the numerical simulations. For clarity, all the presented measurements are corrected by the numerical temperature to be representative of the total number density of OH($X^2\Pi_i$).

3. Numerical modeling

Large Eddy Simulations (LES) of the turbulent flame and the NRP discharges are performed with YALES2, an unstructured finite-volume low-Mach number code dedicated to high-performance computing of reactive flows [58]. The sub-grid Reynolds stresses tensor is closed using the dynamic Smagorinsky model [59]. Methane-air combustion chemistry is computed with the LU19 mechanism, involving 19 species and 184 reactions [60]. The LES species balance equations are computed using the Thickened Flame model for LES (TFLES) [61] and the Charlette sub-grid scale flame wrinkling model [62]. Details regarding the numerical setup, including computational domain, mesh, and boundary conditions are given in [38,39,63].

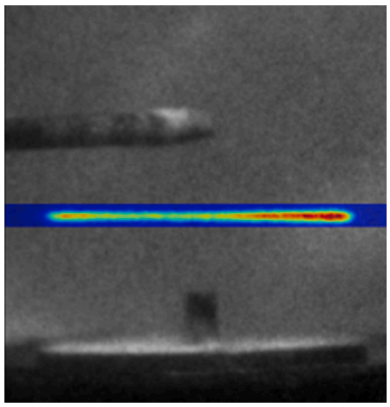

Fig. 8. Picture of the Mini-PAC burner taken with an ICCD camera (black and white) with a non-saturated LIF signal superimposed (false colors).

The thermochemical effects of nanosecond discharges on combustion are described by the model of Castela et al. [36]. This phenomenological model is based on the observation that the main effects of nanosecond discharges in air are fast gas heating and fast dissociation of oxygen molecules at the nanosecond scale, and slow gas heating at the microsecond scale. The strength of this model is to partition the discharge energy between these three effects, allowing to capture them at a low-CPU cost. The additional term of fast gas heating and the species production rates due to plasma kinetics are closed by analytical expressions based on the experimental and numerical characterization of NRP discharges [11,64,65]. In addition to the filtered Navier-Stokes and species equations, the YALES2 code solves a balance equation for an effective vibrational energy used to emulate a slow gas heating with a process similar to vibrational-translational relaxation. Details are given in [36]. Finally, the discharge is assumed to be a cylinder of length 5 mm and radius 0.6 mm, as inferred from experimental discharge imaging.

4. Cumulative effects of NRP discharges: comparisons of experiments and simulations of flame stabilization

As mentioned before, the reference experiment is a challenging case because it involves both the transient regime from the initial unstable flame to the stable flame, as well as the steady-state regime. Initially (without plasma), the flame is near the lean blow-off limit and is confined to the recirculation zone downstream of the bluff body. A significant fraction of the gas is not burnt, as can be seen in Fig. 2. A burst of 5000 discharge pulses is then applied to this weak flame, and the flame becomes significantly enhanced. The transient regime from the weak flame to the stabilized flame and the steady-state regime are experimentally characterized and compared with numerical LES results obtained with the model of Castela et al.

4.1. Electrical characterization of the burst of discharges

The pulse generator was set to a fixed voltage in all following experiments. However, because of pulser peculiarities, the energy deposited by the first few discharges differed slightly from the energy deposited by discharges in the steady-state regime. Fig. 9 shows the peak voltage and current of the incident pulse for the first 10 discharges and

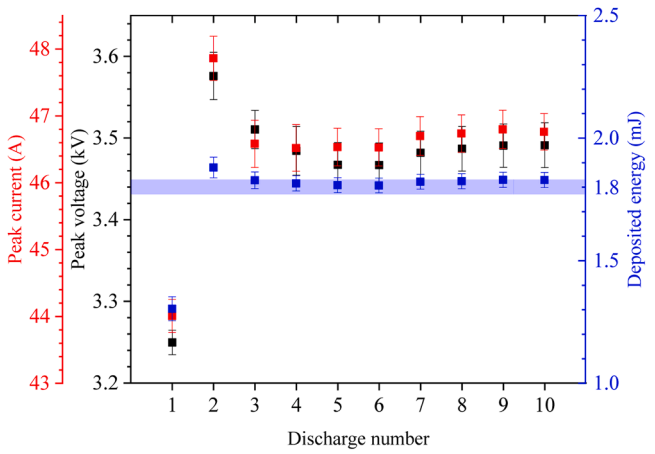

Fig. 9. Evolution of incident peak voltage, peak current, and total deposited energy for the first 10 discharges of the burst. The blue strip corresponds to an energy of 1.8 ± 0.03 mJ. Data are obtained from an average of 10 000 samples, and the error bars correspond to one standard deviation.

the total energy deposited by these discharges. The first pulse exhibits a voltage undershoot, resulting in an energy deposition of 1.3 mJ. Conversely, the second pulse exhibits a slight voltage overshoot. Starting from the third pulse, the incident pulse amplitude is very stable, and the deposited energy reaches the steady-state value of 1.8 mJ. For consistency, the numerical simulations account for these variations of discharge energy.

4.2. Flame shape development during the burst of discharges

As presented in Fig. 2, the weak flame without plasma is confined to the recirculation zone of the bluff body and barely spans two bluff-body diameters in length downstream. However, when NRP discharges are applied, the flame grows and stabilizes even though the bulk velocity of the flow is high.

In Refs. [44,54], the discharge emission was characterized at steady state (i.e., with discharges applied continuously at 20 kHz). In this work, we study the transient stabilization mechanism. The transition from the weak flame without plasma to the plasma-stabilized flame is illustrated in Fig. 10 with Abel-inverted average OH* chemiluminescence images. The first image corresponds to the weak flame without discharge. The following images present the flame shape evolution during the burst of

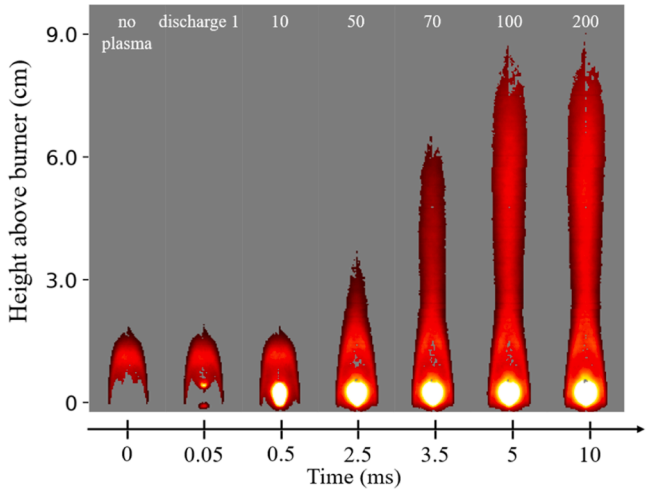

Fig. 10. Abel-inverted average OH* chemiluminescence images of the flame evolution under the effect of the burst of discharges.

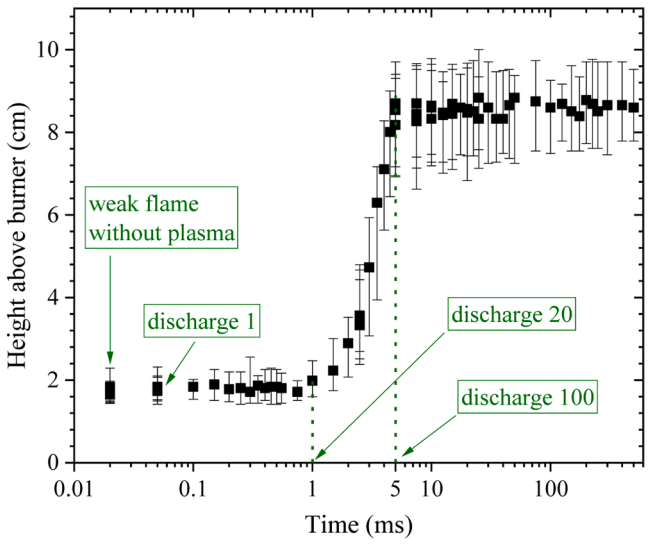

Fig. 11. Flame height above burner during the burst of discharges. The height is determined from Otsu's contours of Abel-inverted average OH* chemiluminescence images. Each datapoint is the average of 1000 samples, and the error bars correspond to the standard deviation.

discharges. The flame contour is defined by the intensity threshold obtained with Otsu's method [66] applied to the image of the weak flame without plasma. This threshold value is then used to delineate the flame contour of all images and to compute the flame Height Above the Burner (HAB), whose evolution is plotted in Fig. 11.

For $t < 1$ ms (i.e., until discharge 20), Fig. 10 shows that the plasma does not affect the flame shape. Even though there is no macroscopic effect on the flame shape during this time interval, the OH* chemiluminescent intensity strongly increases in the recirculation zone, indicating substantial chemical and thermal activity. The flame starts to grow approximately after $t = 1$ ms, which corresponds to the time response of the flame to the application of NRP discharges. Then, the flame develops until reaching the steady-state regime at about $t = 5$ ms, which corresponds to 100 discharges (see Figs. 10 and 11).

The numerical analysis in Ref. [39] showed that O radicals generated by the NRP discharges promote the production of reactive species (mainly OH, O_2, and H_2). This chemical activity corroborates the progressive increase in OH* chemiluminescence in the recirculation zone, between $t = 0$ and $t = 0.5$ ms. In a previous study, Particle Imaging Velocimetry measurements showed that the residence time in the recirculation zone for an air flowrate of 15 Nm^3/h (comparable with the 17.3 Nm^3/h of the present experiment) is about 0.8 ms [67]. Through planar LIF imaging, Xu et al. [68] showed that OH radicals are produced in the discharge region and, because of their long lifespan, are advected toward the flame front at the edges of the bluff body where the shear layer between the burnt gases and the fresh gases is located. This effect causes a substantial increase in the methane consumption rate by the flame front surrounding the recirculation zone (4 mm $\leq r \leq$ 5 mm). As discussed by the authors of Ref. [39], the numerical simulations showed that the gain in flame thermal power was about 2 when applying NRP discharges. They further provided a detailed analysis showing that 70 % of this gain can be explained by the increase of the flame surface and 30 % by the exothermic reactions of the discharge products with the fresh gases in the shear layers around the recirculation zone.

The development of the flame downstream the recirculation zone results from competitive vorticity generation mechanisms in the wake of the bluff body. Without plasma, the vorticity generated by the shear layer of the bluff body tends to extinguish the flame [69]. In the present study, since we are near lean blow-off, the vorticity confines the combustion to the recirculation zone downstream of the bluff body. In the case of a reacting flow, the exothermicity tends to generate vorticity of

the opposite sign, which enables the flame to open and propagate outside the recirculation zone, according to Shanbhogue *et al.* [69].

Therefore, the flame dynamics can be explained by the combined effects of (i) the recirculation of reactive species produced by the discharges and the improved heat release, and (ii) the vorticity generation. The flame front spreads further downstream from the bluff body, allowing consumption of the fresh gases not burnt without plasma and stabilization of the flame.

Fig. 12 shows the measured OH* chemiluminescence integrated over the field of view (obtained from images of the flames not Abel-inverted). The burst of discharges starts at $t = 0$ ms. As was shown in Ref. [70], the OH* chemiluminescence intensity can be used as a marker of the heat release rate in premixed methane-air flames at atmospheric pressure. We thus compare in Fig. 12 the measured temporal evolution of the OH* chemiluminescence (blue squares) with the computed heat release rate of the flame with (red line) and without (black line) NRP discharges. The experimental results are averaged over 1000 bursts, whereas the simulations correspond to a single burst of pulses. The temporal fluctuations of the numerical results are due to turbulence, as confirmed by the fluctuations of the thermal power of the weak flame without plasma (black line). Fig. 12 shows that the temporal evolution of the OH* chemiluminescence follows the same trend as the simulated increase in flame power, both reaching steady state about 7 ms after the start of the burst. Thus, the LES simulations qualitatively capture the temporal dynamics of the plasma-assisted flame.

For the weak flame without NRP discharges, Fig. 13 shows a comparison between i) the experimental Abel-inverted image of the average OH* chemiluminescent intensity, ii) two instantaneous experimental snapshots of the OH* emission, and iii) a time-instant solution of the heat release in the centerline plane from the LES simulation. Pockets of combustion downstream of the weak flame are observed in the experimental snapshots and the time-instant LES simulation. However, these pockets are not seen in the Abel-inverted image obtained from an average of 1000 single-shot images because these events are rare and occur at different positions.

In Fig. 14, the same experimental and numerical results are presented but for the flame assisted by NRP discharges. Compared to the non-assisted case, the flame volume is significantly increased. Strictly speaking, the line-of-sight integrated OH* signal cannot be directly compared to a 2D slice of the numerical flame heat release. In addition,

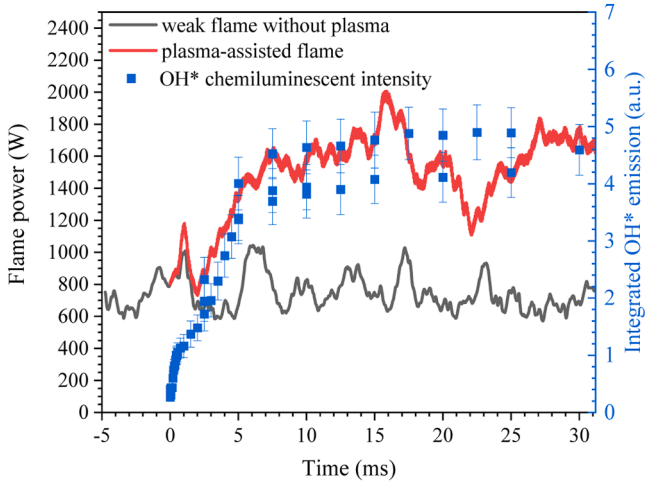

Fig. 12. Comparison of the numerical flame power of the non-assisted flame (black line) and of the plasma-assisted flame (red line) to the experimental OH* chemiluminescent intensity integrated over the whole image for each discharge of the burst (blue squares). Experimental data are obtained from an average of 1000 samples, and the error bars correspond to the standard deviation. Duplicate points correspond to measurements taken on different days. The burst of discharges starts at $t = 0$ ms.

because of the chaotic nature of the turbulence, a direct comparison of instantaneous quantities in a turbulent flame is not consistent. Note that because of CPU time restrictions, it was not possible to perform a significant number of simulations to obtain averaged results. Still, these figures qualitatively show that the NRP discharges impact similarly the flame shape and length in both experiments and simulations.

4.3. Temperature evolution during the burst of discharges

Fig. 15(a) shows the measured gas temperature evolution at mid-gap during the first 5000 discharges. We only plot the temperature at the very beginning of each pulse (i.e., at time $t = 2$ ns). As mentioned before (see Fig. 6), most of the gas heating occurs by the end of the discharge and after the discharge during the quenching phase [11], and the gas temperature remains constant during the first few nanoseconds of the discharge. Therefore, the measured temperature provides the gas temperature immediately before the pulse using Eq. (2), and it gives a good indication of the lower envelope of the temperature evolution during the burst.

The temperature measured at the beginning of the 1st discharge is consistent with the flame adiabatic flame temperature without plasma (1992 K at an equivalence ratio of 0.8). Because of the low energy deposited by the 1st discharge (1.3 mJ), the temperature measured at the beginning of the 2nd discharge is almost unchanged. The pre-pulse temperature increases then by 1250 K between the 3rd (t = 150 μs) and the 10th discharge (t = 500 μs). After approximately 10 to 20 discharges, the heating produced by each pulse, and the subsequent exothermic reactions in the interelectrode gap is balanced by convection and diffusion. A steady state pulsing regime is then reached. Similar cumulative heating effects were observed in air for discharges applied from 1 to 250 kHz by Adams et al. [71], and also in air and methane-air for discharges applied from 1 to 30 kHz in [72,73]. They showed that the temperature plateauing value increases with the discharge repetition frequency. The increase of temperature is due to the ultrafast heating effect and the corroborated exothermic reactions induced by the species generated by the NRP discharge. The relative importance of each effect on the temperature increase will be explored in future work.

Fig. 15(b) compares the measured and simulated gas temperatures. The black squares correspond to the temperature measurements, and the computed temperature evolution is shown by the red solid line. The numerical results evidence the ultra-fast gas heating induced by each NRP discharge. Subsequently to each pulse, the gas temperature increases by about 1000 K due to ultrafast heating and then decays due to the convection and diffusion of hot gases. As can be seen in Fig. 15(b), the pulse-to-pulse evolution of the gas temperature is very well captured by the simulations. Remarkable agreement is obtained for both the evolution during the transient phase (first 10 discharges) and the steady-state temperature.

The characteristic time scale of the temperature evolution, about 0.5 to 1 ms in both the experiments and the simulations, suggests that about 10 to 20 pulses are enough to reach the steady-state temperature regime. Thanks to the cumulative effects of the discharges, operating with bursts of 10 pulses might be sufficient to produce a stabilization effect similar to the case with the discharges applied continuously. Operation of the discharges in duty cycle could then reduce the overall energy cost. We have shown in other configurations that the introduction of a duty cycle reduces the electrical power of the NRP discharges by 30 % in Ref. [49], and by a factor of 4 in Ref. [15], while maintaining a similar LBO limit extension as with continuously applied pulses.

4.4. OH evolution during the burst of discharges

Fig. 16 shows the radial OH fluorescence profiles obtained in the middle of the interelectrode gap. These measurements are averaged 100 times for each profile. In the weak flame without discharge (black squares), the fluorescence intensity is minimal on the axis of the

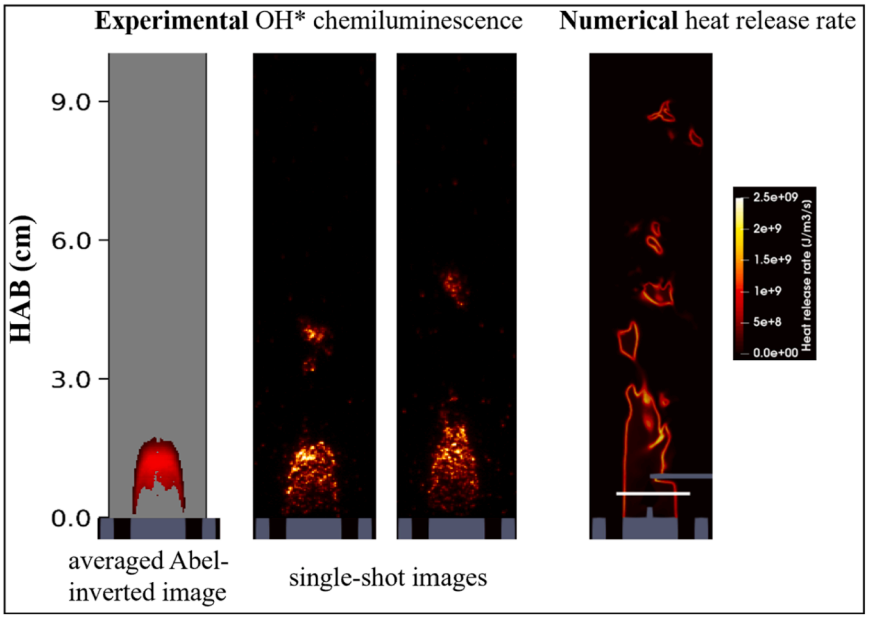

Fig. 13. Comparison of average Abel-inverted and single-shot experimental OH* chemiluminescence images with cross-sectional view of instantaneous numerical heat release rate without plasma. The same length scale is used for experimental and numerical images. The numerical OH profiles presented in Section 4.4 are extracted along the white line.

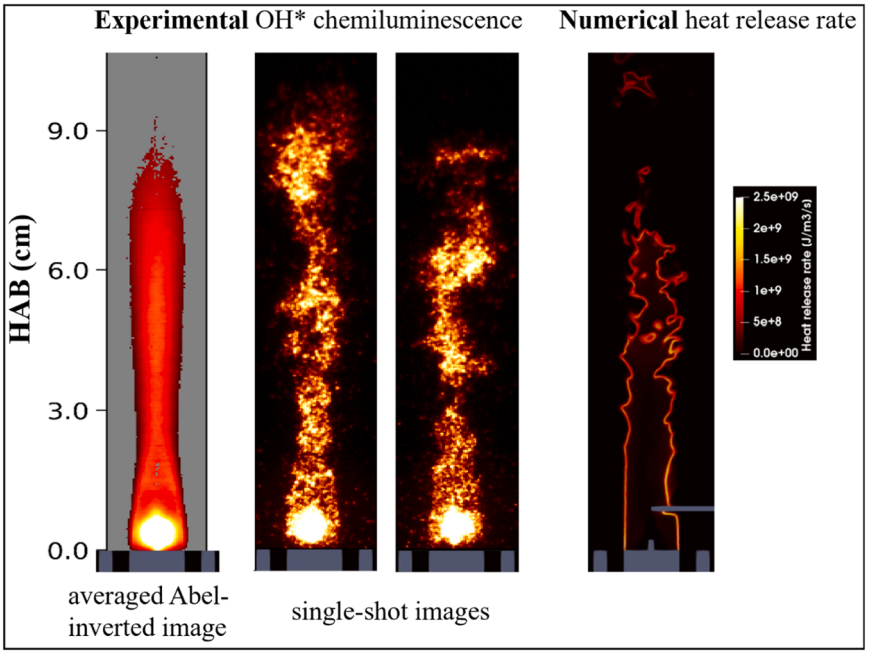

Fig. 14. Comparison of average Abel-inverted and single-shot experimental OH* chemiluminescence images with cross-sectional view of instantaneous numerical heat release rate with discharges applied continuously for the experimental case, and at t = 15 ms (i.e., after 300 discharges) for the numerical case.

interelectrode gap ($r = 0$ mm) and maximal close to the shear layer where the burnt gases ignite the fresh gases and where the flame front is localized ($r = \pm 4$ mm). The profile of the 1st discharge (red squares) shows that the OH number density increases on the discharge axis. Then, after the 2nd and 3rd discharges, the OH profiles keep increasing and widening from pulse to pulse until discharge 15 (yellow squares). After discharge 15 the OH number density at $r = 0$ mm reaches steady state. A large amount of OH radicals is thus produced in the recirculation zone with a sevenfold increase on the discharge axis.

OH is produced directly by the discharge via the dissociation of H_2O or via subsequent reactions with atomic oxygen or hydrogen. It is also possible that OH is produced locally due to the temperature rise in the recirculation zone. OH molecules are then convected towards the shear layer and fill the entire recirculation zone.

Fig. 16 compares the simulated OH profiles with the corrected fluorescence profiles. As the OH-LIF experiments were not calibrated in intensity, we used the numerical results of the non-assisted flame to obtain a scaling factor that was then applied to all time delays (see Section 2.5). The scale of the fluorescence signal in the figure is adjusted to match the OH number density of the non-assisted flame obtained with the numerical simulation at $r = \pm 4$ mm, which corresponds to the flame front. While experimental data correspond to ensemble-averaging, the

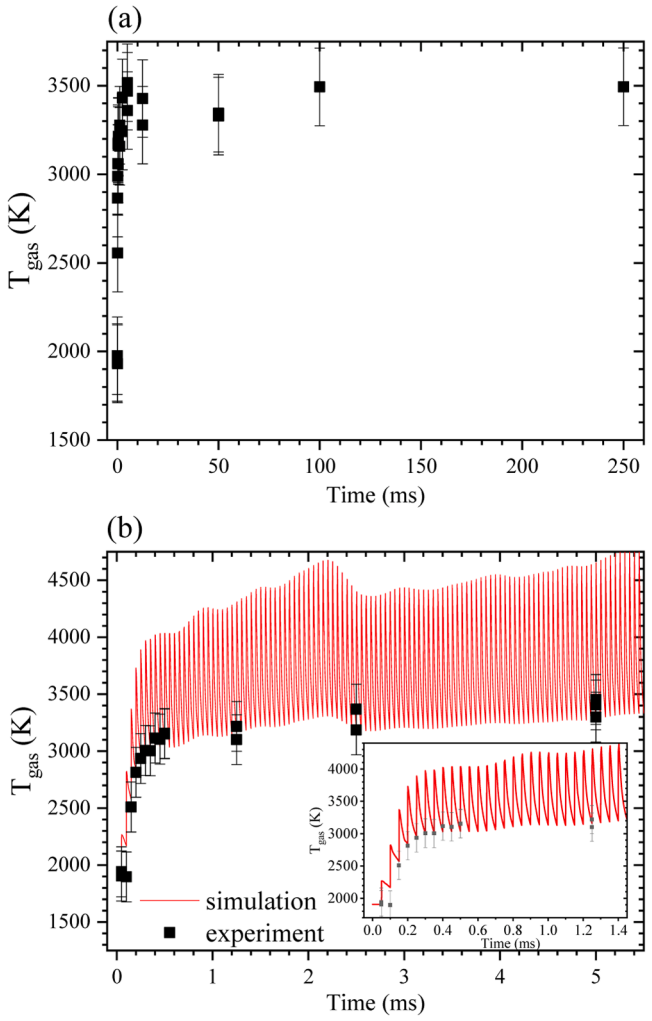

Fig. 15. (a) Evolution of the gas temperature deduced from the rotational temperature of N_2(C) at the beginning of each of the first 5000 discharges. Duplicate points correspond to measurements taken on different days. (b) Comparison of the experimental (black symbols) and numerical (red line) temperature evolutions in the discharge region during the stabilization sequence. The inset shows the data for the first discharges.

numerical data correspond to a single simulation because of computational cost constraints. The profiles present some asymmetry likely due to turbulence and to the hydrodynamic effects of the discharges [74,75]. The OH profile of the non-assisted flame perfectly matches the simulated profile. The OH profile is also well predicted after the 1st discharge. The numerical profiles of the 2nd and 3rd discharges slightly underestimate the fluorescence profiles. The numerical and experimental profiles of the 5th discharge agree remarkably well. After the 10th discharge, the overall agreement remains satisfactory, but the numerical OH density is slightly overestimated on the discharge axis and underestimated on the sides. One explanation could be that the nanosecond discharge model of Castela *et al.* only accounts for O production via dissociation of O_2. It does not account for the radicals produced by the discharge-induced dissociation of the burnt gases (CO_2 and H_2O). An extension of this model, accounting for plasma discharge effects on gases other than O_2 and including NO formation, has been developed [48] and will be presented in future work. Nevertheless, the model of Castela et al. is found to produce OH profiles in reasonable agreement with the experiments. Moreover, the simulations well capture the dynamics: as in the experiments, steady state is reached in the interelectrode gap after 10 to 20

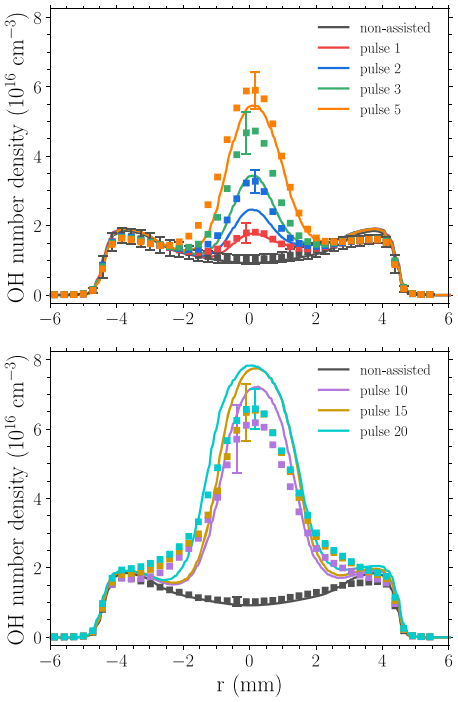

Fig. 16. Comparison of the experimental radial profiles of OH density measured 45 μs after each discharge in the middle of the interelectrode gap (squares) to the numerical OH number density profiles at the same time and location (solid lines) during the stabilization sequence. Error bars correspond to the standard deviation of the measurements.

discharges (0.5 to 1 ms). This time scale also matches the period required to match the thermal steady state in the interelectrode gap.

5. Conclusions

We presented in this work an experiment designed to challenge plasma-assisted combustion simulations of turbulent flames and NRP discharges. In a bluff-body burner, a burst of 5000 NRP discharges was applied at 20 kHz in a lean-premixed turbulent methane-air flame initially near the lean blow-off limit. The stabilization process was first studied by OH* chemiluminescence to characterize the flame shape evolution. The stabilization time scale was found to be comparable with the residence time of about 1 ms in the recirculation zone downstream of the bluff body. The thermal and chemical cumulative effects of NRP discharges were thoroughly characterized in both the transient and steady-state regimes. The temperature evolution in the discharge region was measured by OES during the burst of discharges and showed a similar characteristic time scale of about 1 ms. The temperature surge in the discharge region due to the cumulative heating of the discharges is about 1250 K. The evolution of the OH profile in the recirculation zone exhibits dynamics very similar to the gas temperature. Compared to the non-assisted flame, applying NRP discharges induces a sevenfold increase in the OH number density in the discharge gap.

This reference experimental data set was then compared with LES performed with the nanosecond discharge model of Castela *et al.* This model, based on the knowledge of nanosecond discharge effects in air, has the great advantage of avoiding computationally expensive detailed plasma kinetics. Flame dynamics are very well captured by the simulations. The temperature and OH profiles measured in the discharge region agree remarkably well with the experiments. Both the transient and steady-state regimes are well reproduced. This shows that the simulation is able to predict the cumulative thermal and chemical effects of NRP discharges on the flame. Therefore, the model of Castela et al. is validated against quantitative experimental data.

Finally, this work, along with the work of Malé et al. [12] and Bechane [63], demonstrates that using a simplified model of nanosecond discharges in LES of turbulent flames is a very promising numerical tool for the design of plasma-assisted combustion applications.

Novelty and significance

This work is novel and significant because it provides the first quantitative comparisons of experiments and 3D numerical simulations of the dynamic process of plasma-assisted stabilization by nanosecond discharges of a lean turbulent flame at atmospheric pressure. The excellent agreement obtained for the quantitative comparisons of OH number density, gas temperature, and flame shapes validates the Large Eddy Simulation using the phenomenological model of nanosecond discharges introduced by Castela *et al.* This demonstrates that coupling a simplified model of nanosecond discharges to a high-fidelity combustion solver is a relevant approach for plasma-assisted combustion simulations. In addition, the experimental data will be useful to test and validate other numerical models of plasma-assisted combustion.

Data availability

The data that support the findings of this study are publicly available: https://doi.org/10.57745/RFMXL4.

CRediT authorship contribution statement

Victorien P. Blanchard: Writing – review & editing, Writing – original draft, Visualization, Validation, Methodology, Investigation, Formal analysis, Data curation, Conceptualization. **Yacine Bechane:** Writing – original draft, Visualization, Validation, Methodology, Investigation, Formal analysis, Data curation, Conceptualization. **Nicolas Q. Minesi:** Writing – review & editing, Writing – original draft, Visualization, Validation, Methodology, Investigation, Formal analysis, Data curation, Conceptualization. **Stéphane Q.E. Wang:** Validation. **Benoît Fiorina:** Writing – review & editing, Writing – original draft, Validation, Supervision, Project administration, Funding acquisition, Formal analysis, Conceptualization. **Christophe O. Laux:** Writing – review & editing, Writing – original draft, Validation, Supervision, Project administration, Methodology, Funding acquisition, Formal analysis, Conceptualization.

Declaration of competing interest

The authors declare that they have no known competing financial interests or personal relationships that could have appeared to influence the work reported in this paper.

Acknowledgments

This work has received funding from the Agence Nationale de la Recherche (PASTEC grant ANR16-CE22–0005) and the European Research Council (ERC) under the European Union's Horizon 2020 research and innovation program (GreenBlue grant agreement No.101021538). Dr. Nicolas Minesi was supported by the IDEX PhD fellowship ANR-11-IDEX-003–02. This work was granted access to the HPC resources from IDRIS, TGCC and CINES under the allocation A0052B10253 made by GENCI (Grand Equipement National de Calcul Intensif) and HPC resources from the Mesocentre computing center of CentraleSupelec and Ecole Normale Supérieure Paris-Saclay supported by CNRS and Région Ile-de-France (http://mesocentre.centralesupelec.fr/). We acknowledge PRACE for awarding us access to Joliot-Curie at GENCI@CEA, France. The authors would like to thank Cécile Oriot for the photographs of Fig. 2, Erika Jean-Bart, and Yannick Le Teno for technical assistance with the Mini-PAC burner.

References

[1] International Energy Agency, World Energy Outlook 2022, 2022.
[2] Y. Huang, V. Yang, Dynamics and stability of lean-premixed swirl-stabilized combustion, Prog. Energy Combust. Sci. 35 (2009) 293–364, https://doi.org/10.1016/j.pecs.2009.01.002.
[3] A. Starikovskiy, N. Aleksandrov, Plasma-assisted ignition and combustion, Prog. Energy Combust. Sci. 39 (2013) 61–110, https://doi.org/10.1016/j.pecs.2012.05.003.
[4] S.M. Starikovskaia, Plasma-assisted ignition and combustion: nanosecond discharges and development of kinetic mechanisms, J. Phys. D Appl. Phys. 47 (2014) 353001, https://doi.org/10.1088/0022-3727/47/35/353001.
[5] Y. Ju, W. Sun, Plasma assisted combustion: dynamics and chemistry, Prog. Energy Combust. Sci. 48 (2015) 21–83, https://doi.org/10.1016/j.pecs.2014.12.002.
[6] C.H. Kruger, C.O. Laux, L. Yu, D.M. Packan, L. Pierrot, Nonequilibrium discharges in air and nitrogen plasmas at atmospheric pressure, Pure Appl. Chem. 74 (2002) 337–347, https://doi.org/10.1351/pac200274030337.
[7] D.Z. Pai, D.A. Lacoste, C.O. Laux, Nanosecond repetitively pulsed discharges in air at atmospheric pressure—The spark regime, Plasma Sources Sci. Technol. 19 (2010) 065015, https://doi.org/10.1088/0963-0252/19/6/065015.
[8] C.O. Laux, Applications of plasma discharges to combustion, J. Combust. Soc. Jpn 64 (2022) 257–264, https://doi.org/10.20619/jcombsj.64.209_257.
[9] M. Uddi, N. Jiang, E. Mintusov, I.V. Adamovich, W.R. Lempert, Atomic oxygen measurements in air and air /fuel nanosecond pulse discharges by two photon laser induced fluorescence, Proc. Combust. Inst. 32 (2009) 929–936, https://doi.org/10.1016/j.proci.2008.06.049.
[10] T. Ombrello, S.H. Won, Y. Ju, S. Williams, Flame propagation enhancement by plasma excitation of oxygen. Part II: effects of O2(a1Dg), Combust. Flame 157 (2010) 1916–1928, https://doi.org/10.1016/j.combustflame.2010.02.004.
[11] D.L. Rusterholtz, D.A. Lacoste, G.D. Stancu, D.Z. Pai, C.O. Laux, Ultrafast heating and oxygen dissociation in atmospheric pressure air by nanosecond repetitively pulsed discharges, J. Phys. D Appl. Phys. 46 (2013) 464010, https://doi.org/10.1088/0022-3727/46/46/464010.
[12] Q. Malé, S. Shcherbanev, N. Noiray, Numerical study of plasma assisted combustion in a sequential combustor, Proc. Combust. Inst. (2022) 1–9, https://doi.org/10.1016/j.proci.2022.06.016.
[13] N.A. Popov, Kinetics of plasma-assisted combustion: effect of non-equilibrium excitation on the ignition and oxidation of combustible mixtures, Plasma Sources Sci. Technol. 25 (2016) 043002, https://doi.org/10.1088/0963-0252/25/4/043002.
[14] G. Pilla, D. Galley, D.A. Lacoste, F. Lacas, D. Veynante, C.O. Laux, Stabilization of a turbulent premixed flame using a nanosecond repetitively pulsed plasma, IEEE Trans. Plasma Sci. 34 (2006) 2471–2477, https://doi.org/10.1109/TPS.2006.886081.
[15] V.P. Blanchard, P. Scouflaire, C.O. Laux, S. Ducruix, Combustion performance of plasma-stabilized lean flames in a gas turbine model combustor, Applicat. Energy and Combust. Sci. 15 (2023) 100158, https://doi.org/10.1016/j.jaecs.2023.100158.
[16] C.A. Pavan, C. Guerra-Garcia, Nanosecond pulsed discharge dynamics during passage of a transient laminar flame, Plasma Sources Sci. Technol. 31 (2022) 115016, https://doi.org/10.1088/1361-6595/aca0bc.
[17] J. Choe, W. Sun, Blowoff hysteresis, flame morphology and the effect of plasma in a swirling flow, J. Phys. D Appl. Phys. 51 (2018) 365201, https://doi.org/10.1088/1361-6463/aad4dc.
[18] G. Vignat, N. Minesi, P.R. Soundararajan, D. Durox, A. Renaud, V. Blanchard, C. O. Laux, S. Candel, Improvement of lean blow out performance of spray and premixed swirled flames using nanosecond repetitively pulsed discharges, Proc. Combust. Inst. 38 (2021) 6559–6566, https://doi.org/10.1016/j.proci.2020.06.136.
[19] S. Barbosa, G. Pilla, D.A. Lacoste, P. Scouflaire, S. Ducruix, C.O. Laux, D. Veynante, Influence of nanosecond repetitively pulsed discharges on the stability of a swirled propane/air burner representative of an aeronautical combustor, Philos. Trans. R. Soc., A 373 (2015) 20140335, https://doi.org/10.1098/rsta.2014.0335.
[20] F. Di Sabatino, D.A. Lacoste, Enhancement of the lean stability and blow-off limits of methane-air swirl flames at elevated pressures by nanosecond repetitively pulsed discharges, J. Phys. D Appl. Phys. 53 (2020) 355201, https://doi.org/10.1088/1361-6463/ab8f54.
[21] V.P. Blanchard, F. Roqué, P. Scouflaire, C.O. Laux, S. Ducruix, Stabilization of lean flames with nanosecond discharges in a gas turbine model combustor, AIAA SciTech Forum 2023 (2023) 2023–2387, https://doi.org/10.2514/6.2023-2387.
[22] G. Heid, G. Pilla, R. Lecourt, D.A. Lacoste, Assisted combustion of an air-kerosene mixture by nanosecond repetitively pulsed discharges, Isabe (2009) 474.
[23] M. Uddi, N. Jiang, I.V. Adamovich, W.R. Lempert, Nitric oxide density measurements in air and air/fuel nanosecond pulse discharges by laser induced fluorescence, J. Phys. D Appl. Phys. 42 (2009) 075205, https://doi.org/10.1088/0022-3727/42/7/075205.
[24] J.K. Lefkowitz, P. Guo, A. Rousso, Y. Ju, Species and temperature measurements of methane oxidation in a nanosecond repetitively pulsed discharge, Philos. Trans. R. Soc., A 373 (2015) 20140333, https://doi.org/10.1098/rsta.2014.0333.

[25] Z. Yin, A. Montello, C.D. Carter, W.R. Lempert, I.V. Adamovich, Measurements of temperature and hydroxyl radical generation/decay in lean fuel-air mixtures excited by a repetitively pulsed nanosecond discharge, Combust. Flame 160 (2013) 1594–1608, https://doi.org/10.1016/j.combustflame.2013.03.015.

[26] I. Shkurenkov, I.V. Adamovich, Energy balance in nanosecond pulse discharges in nitrogen and air, Plasma Sources Sci. Technol. 25 (2016), https://doi.org/10.1088/0963-0252/25/1/015021.

[27] I.V. Adamovich, T. Li, W.R. Lempert, Kinetic mechanism of molecular energy transfer and chemical reactions in low-temperature air-fuel plasmas, Philos. Trans. R. Soc., A 373 (2015) 20140336, https://doi.org/10.1098/rsta.2014.0336.

[28] N.A. Popov, Pulsed nanosecond discharge in air at high specific deposited energy: fast gas heating and active particle production, Plasma Sources Sci. Technol. 25 (2016) 044003, https://doi.org/10.1088/0963-0252/25/4/044003.

[29] I.V. Adamovich, I. Choi, N. Jiang, J.H. Kim, S. Keshav, W.R. Lempert, E. Mintusov, M. Nishihara, M. Samimy, M. Uddi, Plasma assisted ignition and high-speed flow control: non-thermal and thermal effects, Plasma Sources Sci. Technol. 18 (2009), https://doi.org/10.1088/0963-0252/18/3/034018.

[30] A.A. Tropina, M. Uddi, Y. Ju, On the effect of nonequilibrium plasma on the minimum ignition energy: part 2, IEEE Trans. Plasma Sci. 39 (2011) 3283–3287, https://doi.org/10.1109/TPS.2011.2160570.

[31] W. Sun, M. Uddi, S.H. Won, T. Ombrello, C. Carter, Y. Ju, Kinetic effects of non-equilibrium plasma-assisted methane oxidation on diffusion flame extinction limits, Combust. Flame 159 (2012) 221–229, https://doi.org/10.1016/j.combustflame.2011.07.008.

[32] M.S. Bak, M.A. Cappelli, Numerical studies of nitric oxide formation in nanosecond-pulsed discharge-stabilized flames of premixed methane/air, Philos. Trans. R. Soc., A 373 (2015) 20140331, https://doi.org/10.1098/rsta.2014.0331.

[33] F. Tholin, D.A. Lacoste, A. Bourdon, Influence of fast-heating processes and O atom production by a nanosecond spark discharge on the ignition of a lean H2-air premixed flame, Combust. Flame 161 (2014) 1235–1246, https://doi.org/10.1016/j.combustflame.2013.11.007.

[34] X. Mao, H. Zhong, Y. Ju, 2D modeling of plasma-assisted H2-air ignition in a nanosecond discharge with detailed chemistry, AIAA SciTech 2021 Forum (2021), https://doi.org/10.2514/6.2021-1790, 2021–1790.

[35] M.S. Bak, H. Do, M.G. Mungal, M.A. Cappelli, Plasma-assisted stabilization of laminar premixed methane/air flames around the lean flammability limit, Combust. Flame 159 (2012) 3128–3137, https://doi.org/10.1016/j.combustflame.2012.03.023.

[36] M. Castela, B. Fiorina, A. Coussement, O. Gicquel, N. Darabiha, C.O. Laux, Modelling the impact of non-equilibrium discharges on reactive mixtures for simulations of plasma-assisted ignition in turbulent flows, Combust. Flame 166 (2016) 133–147, https://doi.org/10.1016/j.combustflame.2016.01.009.

[37] M. Castela, S. Stepanyan, B. Fiorina, A. Coussement, O. Gicquel, N. Darabiha, C. O. Laux, A 3-D DNS and experimental study of the effect of the recirculating flow pattern inside a reactive kernel produced by nanosecond plasma discharges in a methane-air mixture, Proc. Combust. Inst. 36 (2017) 4095–4103, https://doi.org/10.1016/j.proci.2016.06.174.

[38] Y. Bechane, B. Fiorina, Numerical investigations of turbulent premixed flame ignition by a series of Nanosecond Repetitively Pulsed discharges, Proc. Combust. Inst. 38 (2021) 6575–6582, https://doi.org/10.1016/j.proci.2020.06.258.

[39] Y. Bechane, B. Fiorina, Numerical analysis of turbulent flame enhancement by nanosecond repetitively pulsed plasma discharges, Proc. Combust. Inst. 39 (2023) 5465–5476, https://doi.org/10.1016/j.proci.2022.07.006.

[40] V.P. Blanchard, N. Minesi, Y. Bechane, B. Fiorina, C.O. Laux, Experimental and numerical characterization of a lean premixed flame stabilized by nanosecond discharges, AIAA SciTech Forum 2022 (2022) 2022–2255, https://doi.org/10.2514/6.2022-2255.

[41] N. Barléon, L. Cheng, B. Cuenot, O. Vermorel, A phenomenological model for plasma-assisted combustion with NRP discharges in methane-air mixtures: PACMIND, Combust. Flame 253 (2023) 112794, https://doi.org/10.1016/j.combustflame.2023.112794.

[42] D.A. Xu, D.A. Lacoste, C.O. Laux, Ignition of quiescent lean propane–air mixtures at high pressure by nanosecond repetitively pulsed discharges, Plasma Chem. Plasma Process. 36 (2016) 309–327, https://doi.org/10.1007/s11090-015-9680-3.

[43] J.K. Lefkowitz, T. Ombrello, An exploration of inter-pulse coupling in nanosecond pulsed high frequency discharge ignition, Combust. Flame 180 (2017) 136–147, https://doi.org/10.1016/j.combustflame.2017.02.032.

[44] N.Q. Minesi, V.P. Blanchard, E. Pannier, G.D. Stancu, C.O. Laux, Plasma-assisted combustion with nanosecond discharges. I: discharge effects characterization in the burnt gases of a lean flame, Plasma Sources Sci. Technol. 31 (2022) 045029, https://doi.org/10.1088/1361-6595/ac5cd4.

[45] Y. Bechane, Simulations Numériques De La Combustion Assistée Par plasma, Ph.D. Thesis dissertation, Université Paris-Saclay, CentraleSupélec, 2022.

[46] N. Minesi, Thermal Spark Formation and Plasma-Assisted Combustion By Nanosecond Repetitive discharges, Ph.D. Thesis dissertation, Université Paris-Saclay, CentraleSupélec, 2020. https://tel.archives-ouvertes.fr/tel-03155208.

[47] V.P. Blanchard, N. Minesi, Y. Bechane, B. Fiorina, C.O. Laux, Experimental and numerical characterization of a lean premixed flame stabilized by nanosecond discharges, AIAA SciTech Forum 2022 (2022) 2022–2255, https://doi.org/10.2514/6.2022-2255.

[48] V.P. Blanchard, Thermochemical Effects of Nanosecond Plasma Discharges on Lean Flame Stabilization, Ph.D. Thesis dissertation, Université Paris-Saclay, CentraleSupélec, 2023.

[49] N. Minesi, Thermal Spark Formation and Plasma-Assisted Combustion By Nanosecond Repetitive discharges, Ph.D. Thesis dissertation, Université Paris-Saclay, CentraleSupélec, 2020.

[50] P.J. Bruggeman, N. Sadeghi, D.C. Schram, V. Linss, Gas temperature determination from rotational lines in non-equilibrium plasmas: a review, Plasma Sources Sci. Technol. 23 (2014), https://doi.org/10.1088/0963-0252/23/2/023001.

[51] A.C. Tibère-Inglesse, S.D. McGuire, C.O. Laux, Inferring gas temperature from N 2 emission via rotational distribution of the N 2 B 3 Π g and C 3 Π u states, Plasma Sources Sci. Technol. 32 (2023) 075018, https://doi.org/10.1088/1361-6595/ace5d1.

[52] C.O. Laux, T.G. Spence, C.H. Kruger, R.N. Zare, Optical diagnostics of atmospheric pressure air plasmas, Plasma Sources Sci. Technol. 12 (2003) 125–138, https://doi.org/10.1088/0963-0252/12/2/301.

[53] Specair 3.0, Available from: www.spectralfit.com.

[54] V.P. Blanchard, N.Q. Minesi, S. Stepanyan, G.-D. Stancu, C.O. Laux, Dynamics of a lean flame stabilized by nanosecond discharges, AIAA SciTech Forum 2021 (2021), https://doi.org/10.2514/6.2021-1700, 2021–1700.

[55] J. Luque, D.R. Crosley, Transition probabilities in the A 2Σ+−X 2Πi electronic system of OH, J. Chem. Phys. 109 (1998) 439–448, https://doi.org/10.1063/1.476582.

[56] R.K. Hanson, R.M. Spearrin, C.S. Goldenstein, Spectroscopy and Optical Diagnostics For Gases, Springer, 2016, https://doi.org/10.1007/9783319232522.

[57] K.P. Huber, G. Herzberg, Molecular Spectra and Molecular Structure, Springer US, Boston, MA, 1979, https://doi.org/10.1007/978-1-4757-0961-2.

[58] V. Moureau, P. Domingo, L. Vervisch, Une algorithmique optimisée pour le supercalcul appliqué à la mécanique des fluides numérique, Comptes Rendus - Mecanique 339 (2011) 141–148, https://doi.org/10.1016/j.crme.2010.12.001.

[59] M. Germano, U. Piomelli, P. Moin, W.H. Cabot, A dynamic subgrid-scale eddy viscosity model, Phys. Fluids A 3 (1991) 1760–1765, https://doi.org/10.1063/1.857955.

[60] T. Lu, C.K. Law, A criterion based on computational singular perturbation for the identification of quasi steady state species: a reduced mechanism for methane oxidation with NO chemistry, Combust. Flame 154 (2008) 761–774, https://doi.org/10.1016/j.combustflame.2008.04.025.

[61] O. Colin, F. Ducros, D. Veynante, T. Poinsot, A thickened flame model for large eddy simulations of turbulent premixed combustion, Phys. Fluids 12 (2000) 1843–1863, https://doi.org/10.1063/1.870436.

[62] F. Charlette, C. Meneveau, D. Veynante, A power-law flame wrinkling model for LES of premixed turbulent combustion Part I: non-dynamic formulation and initial tests, Combust. Flame 131 (2002) 159–180, https://doi.org/10.1016/S0010-2180(02)00400-5.

[63] Y. Bechane, Simulations Numériques De La Combustion Assistée Par plasma, Ph.D. Thesis dissertation, Université Paris-Saclay, CentraleSupélec, 2022.

[64] N.L. Aleksandrov, S.V. Kindysheva, M.M. Nudnova, A.Y. Starikovskiy, Mechanism of ultra-fast heating in a non-equilibrium weakly ionized air discharge plasma in high electric fields, J Phys D Appl Phys 43 (2010) 255201, https://doi.org/10.1088/0022-3727/43/25/255201.

[65] N.A. Popov, Investigation of the mechanism for rapid heating of nitrogen and air in gas discharges, Plasma Phys. Rep. 27 (2001) 940–950.

[66] N. Otsu, A threshold selection method from gray-level histograms, IEEE Transactions on Systems, Man., Adn. Cybernetics 9 (1979) 62–66, https://doi.org/10.1109/TSMC.1979.4310076.

[67] G. Pilla, Etude Expérimentale de La Stabilisation de Flammes Propane-Air De Prémélange par Décharges Nanosecondes Impulsionnelles Répétitives, Ph.D. Thesis dissertation, Ecole Centrale Paris, 2008.

[68] D. Xu, D. Lacoste, C. Laux, Temporal and Spatial Evolution of OH Concentration in a Lean Premixed Propane-Air Flame Assisted by Nanosecond Repetitively Pulsed Discharges, in: 51st AIAA Aerospace Sciences Meeting Including the New Horizons Forum and Aerospace Exposition, 2013, https://doi.org/10.2514/6.2013-895, 2013–0895.

[69] S.J. Shanbhogue, S. Husain, T. Lieuwen, Lean blowoff of bluff body stabilized flames: scaling and dynamics, Prog. Energy Combust. Sci. 35 (2009) 98–120, https://doi.org/10.1016/j.pecs.2008.07.003.

[70] C.S. Panoutsos, Y. Hardalupas, A.M.K.P. Taylor, Numerical evaluation of equivalence ratio measurement using OH* and CH* chemiluminescence in premixed and non-premixed methane-air flames, Combust. Flame 156 (2009) 273–291, https://doi.org/10.1016/j.combustflame.2008.11.008.

[71] S. Adams, J. Miles, T. Ombrello, R. Brayfield, J. Lefkowitz, The effect of inter-pulse coupling on gas temperature in nanosecond-pulsed high-frequency discharges, J. Phys. D Appl. Phys. 52 (2019) 355203, https://doi.org/10.1088/1361-6463/ab27ef.

[72] R. Patel, J. van Oijen, N. Dam, S. Nijdam, Low-temperature filamentary plasma for ignition-stabilized combustion, Combust. Flame 247 (2023) 112501, https://doi.org/10.1016/j.combustflame.2022.112501.

[73] R. Patel, J. van Oijen, S. Nijdam, N. Dam, On pulse-to-pulse coupling in low-temperature filamentary plasma-assisted ignition in methane-air flows, Plasma Sources Sci. Technol. 32 (2023) 065003, https://doi.org/10.1088/1361-6595/acd65c.

[74] S. Stepanyan, J. Hayashi, A. Salmon, G.D. Stancu, C.O. Laux, Large-volume excitation of air, argon, nitrogen and combustible mixtures by thermal jets produced by nanosecond spark discharges, Plasma Sources Sci. Technol. 26 (2017) 22–24, https://doi.org/10.1088/1361-6595/aa5a2b.

[75] S. Lovascio, J. Hayashi, S. Stepanyan, G.D. Stancu, C.O. Laux, Cumulative effect of successive nanosecond repetitively pulsed discharges on the ignition of lean mixtures, Proc. Combust. Inst. 37 (2019) 5553–5560, https://doi.org/10.1016/j.proci.2018.06.029.